9-12-2008

Molecular Nanoscience and Engineering on Surfaces

Willi Auwarter

Agustin Schiffrin

Alexander Weber-Bargioni

Yan Pennec

Andreas Riemann
Western Washington University, andreas.riemann@wwu.edu

See next page for additional authors

Molecular nanoscience and engineering on surfaces

Willi Auwärter*

Departments of Chemistry and Physics and Astronomy,
University of British Columbia,
Vancouver, Canada
Fax: +1 604 822 4750 E-mail: wau@tum.de

Physik Department E20,
Technische Universität München,
D-85748 Garching, Germany

Agustin Schiffrin, Alexander Weber-Bargioni and Yan Pennec

Departments of Chemistry and Physics and Astronomy,
University of British Columbia,
Vancouver, Canada
Fax: +1 604 822 4750

Andreas Riemann

Department of Physics and Astronomy,
University of British Columbia,
Vancouver, Canada
Fax: +1 604 822 4750

Department of Physics and Astronomy,
Western Washington University,
Bellingham, WA 98225-9164, USA

Johannes V. Barth*

Department of Physics and Astronomy,
University of British Columbia,
Vancouver, Canada
Fax: +1 604 822 4750
E-mail: jvb@phas.ubc.ca

Physik Department E20,
Technische Universität München,
D-85748 Garching, Germany
*Corresponding authors

Abstract: Molecular engineering of low-dimensional materials exploiting controlled self-assembly and positioning of individual atoms or molecules at surfaces opens up new pathways to control matter at the nanoscale. Our research thus focuses on the study of functional molecules and supramolecular architectures on metal substrates. As principal experimental tools we employ low-temperature scanning tunnelling microscopy and spectroscopy. Here we review recent studies in our lab at UBC: Controlled manipulation of single CO molecules, self-assembled biomolecular nanogratings on Ag(111) and their use for electron confinement, as well as the organisation, conformation, metalation and electronic structure of adsorbed porphyrins.

Keywords: nanochemistry; self-assembly; scanning tunnelling microscopy; supramolecular engineering; surface chemistry; porphyrin; methionine.

Reference to this paper should be made as follows: Auwärter, W., Schiffrin, A., Weber-Bargioni, A., Pennec, Y., Riemann, A. and Barth, J.V. (2008) 'Molecular nanoscience and engineering on surfaces', *Int. J. Nanotechnol*., Vol. 5, Nos. 9/10/11/12, pp.1171–1193.

Biographical notes: Willi Auwärter is currently a Research Associate at the Technical University Munich. He received his PhD in Physics from the University of Zurich in 2003. Subsequently he worked with a scholarship from the Swiss National Science Foundation as postdoctoral fellow at the University of British Columbia and at the Ecole Polytechnique Fédérale de Lausanne. His research focuses on nanoscale science on surfaces, specifically addressing the geometric and electronic structure of molecular buildings blocks and their self-assembly into supramolecular architectures.

Agustin Schiffrin is a PhD student in Chemistry at the University of British Columbia since 2004. His doctoral research project focuses on the self-assembly of biologically relevant molecules on noble metal surfaces and their characterisation with scanning tunnelling microscopy and complementary X-ray absorption surface science techniques. In 2003, he obtained a Diploma in Physics from the Ecole Polytechnique Fédérale de Lausanne.

Alexander Weber-Bargioni completed his PhD in Physics at the University of British Columbia in 2007. His doctoral research focused on the investigation of porphyrin molecules absorbed on metal surfaces. By means of scanning tunnelling microscopy/spectroscopy he studied their self-assembly to supramolecular nanostructures and their electronic structure on the single molecule scale. He is currently at the Lawrence Berkeley National Laboratories, where he investigates the interaction of light with single molecules. He has an MSc from The University of British Columbia, an MSc from the Portland State University and a Vordiplom/BSc from the University of Konstanz, Germany.

Yan Pennec is a research associate in the Physics and Astronomy Department at the University of British Columbia. After the obtainment of his PhD on the Magnetisation Dynamics of Ultra-Thin Films at the University Joseph Fourier in France, he focused during post-doctoral appointments on the studies of surface science at the University of Alberta and later on at the University of British Columbia. He used the scanning tunnelling microscope as a tool of choice for the investigation of condensed matter down to the atomic scale. His interest covers a large range of topics from semiconductors to oxides to organic materials.

Andreas Riemann is an Assistant Professor at Western Washington University. He previously was a postdoctoral fellow at the University of British Columbia. His postdoctoral research focused on molecular nanostructures on metallic substrates investigated by low-temperature STM. Currently, he is studying functional molecules under ambient conditions with STM and also magnetic multilayer structures using LEED and MOKE. He has a PhD from the Freie Universität Berlin and a Diploma from the Martin-Luther-Universität Halle Wittenberg.

J.V. Barth is presently Adjunct Professor at the Department of Physics and Astronomy at The University of British Columbia and Chair of Experimental Surface Physics at Technische Universität München. Previously he was a Canada Research Chair at UBC and Research Associate, Docent and Visiting Professor at Ecole Polytechnique Fédérale de Lausanne, where he received the Venia Legendi in 1999. He was Postdoctoral Fellow at the IBM Almaden Research Center, San Jose, and at the Fritz-Haber-Institut der Max-Planck-Gesellschaft, Berlin, where he also did his PhD studies with G. Ertl. He obtained a Diploma in Physics from the Ludwig-Maximilians-Universität München. His current main research fields are Molecular Nanoscience and Surface Chemical Physics.

1 Introduction

The handling and control of matter at the atomic and molecular scale is crucial for the advancement of nanoscale science and nanotechnology. The key objective of our research is the control of functional molecules and their embedding in molecular nano-architectures at well-defined substrates. To this end we apply both molecular manipulation techniques and principles from supramolecular science enabling a high degree of structural organisation within the nanoregime [1]. In particular, we employ appropriately designed molecular building blocks for the modular *aufbau* of functional architectures and nanostructures from organic species and metal atoms at well-defined surfaces. Our studies put emphasis on nanochemistry, self-assembly and supramolecular engineering. This work is highly interdisciplinary, integrating aspects from physical nanoscience, supramolecular chemistry, physical chemistry, surface chemistry and physics, and materials research. These activities contribute to the development of novel bottom-up fabrication techniques, functional materials and future device concepts [2–4] (cf. Figure 1).

We concentrate on atomistic studies of both single complex molecular species and organised molecular assemblies by temperature-controlled scanning tunnelling microscopy (STM) and spectroscopy (STS), complementary integral tools and theoretical modelling. STM is a primary experimental tool for the observation and manipulation of matter at the atomic scale and, as such, was instrumental in establishing the field of nanoscience and technology [5]. The unparalleled spatial resolution and versatility of STM provide unique opportunities for the exploration of single molecules [6]. These attributes were enhanced with the full development of molecular manipulation, chemical modification and STS capacities [7]. In the following we provide exemplary illustrations how to use STM for a comprehensive understanding of molecular

recognition and self-assembly at surfaces, and to develop suitable design strategies for novel supramolecular architectures and functional nanosystems.

Figure 1 Two approaches to control matter at the nanoscale. For top-down fabrication, methods such as lithography, writing or stamping define the desired features. Bottom-up techniques exploit self-processes to achieve regular supramolecular architectures from the atomic to the mesosopic scale. Shown (clockwise from top) are a nanomechanical electrometer obtained by electron-beam lithography, patterned films of carbon nanotubes obtained by microcontact printing, a carbon nanotube connecting two electrodes, a nanoporous Fe-carboxylate network obtained by metal-directed assembly, and a 12 Å periodicity superlattice formed by individual Fe atoms on Cu(111) at T = 10 K [8]. Adapted from [3] (for colours see online version)

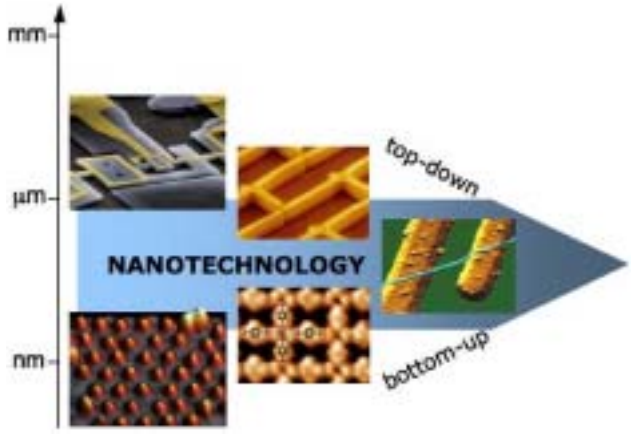

2 Writing with single molecules

The precise manipulation of individual atoms and molecules, made possible by the progress in STM instrumentation and the development of various manipulation procedures, is a most fascinating and relevant task in nanoscale science. It allows not only to structure and modify matter on the atomic scale, but also grants access to basic physical properties of such artificial nanostructures: Highlights include the positioning of single adatoms and molecules [9–14], induced chemical reactions [15], tip-induced field modulation of adsorbed single molecules [16] or conformational changes in large organic molecules [17–21]. These studies open up the possibility to study the interaction of an artificial nanostructure with its surrounding, as demonstrated already in early experiments on the impact of quantum corrals on the surface electronic structure [22] or in more recent experiments focused on the modification of the electronic structure of adsorbates [23], molecule-metal contacts [24–26] or metal chains [27].

While high resolution imaging of surface structures and adsorbates by STM is a standard procedure nowadays, there are still not too many research groups which can rely on instrumentation (apparatus, electronics and software) that fulfils the high requirements necessary for a controlled, reliable and fast manipulation of single adsorbates. Thus, the manipulation experiments of carbon monoxide on a Cu(111) surface presented in this section, are used to demonstrate the capabilities of our low-temperature STM setup. Since the positioning of small molecules by STM on metal surfaces relies on established

procedures [11–13,28–30], the CO/Cu(111) system represents an ideal test case. In addition, CO on Cu(111) represents a marker to determine adsorption sites of other adsorbates (see Section 3.3).

Figure 2(a) shows the Cu(111) surface after a minute exposure to CO dosed in situ at a sample temperature of 18 K. Each depression corresponds to a single CO molecule imaged with a bare metal tip. This inverted contrast is well explained by different tunnelling channels between sample, molecule and tip [31,32]. It is interesting to note that picking up a CO molecule by vertical manipulation changes the imaging mechanism completely [13]: CO molecules are now imaged as sombrero shaped protrusions (see Figure 2(b)). Additionally, the CO functionalised tips guarantee an increased resolution.

Figure 2 Controlled manipulation of single CO molecules by the STM. (a) Randomly distributed CO molecules deposited on Cu(111) at 18 K. Imaged by a metal tip, the CO molecules appear as depressions. (b) Picking up a single molecule by applying a vertical manipulation procedure results in an inverted contrast. (c) Tip trajectory during a manipulation of a CO molecule over 3 nm. Each saw tooth segment represents a jump from one substrate lattice site to the next (approximately 2.5 Å). (d) Snapshots during the writing of the letters CFI by lateral manipulation. A movie displaying the complete assembly process is accessible at http://www.phas.ubc.ca/~stm. (e) The final result: Every blue spot represents a single CO molecule adsorbed on an 'on top' site of the Cu lattice. The letters are a mere 2 nm wide (for colours see online version)

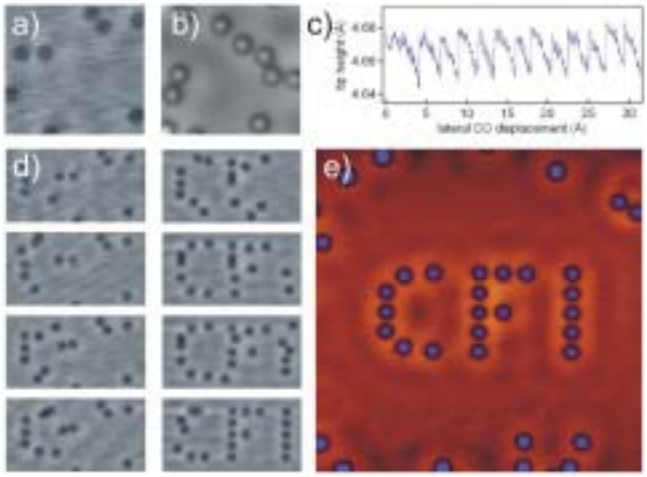

In order to assemble artificial CO structures we applied a lateral manipulation procedure, where the molecule is moved by interactions with the STM tip. A typical manipulation includes the following steps:

- The tip is positioned behind the target molecule and approached close to the surface by applying small bias voltages (50 mV) and large tunnelling currents (80 nA).
- The tip is translated along a line towards the desired final position. Short range forces between the CO and the tip induce sudden hops of the molecule. These jumps from one lattice site to the next can be observed in the tip height. Figure 2(c) shows the saw tooth trajectory of the vertical tip position while a CO molecule was moved over 12 lattice sites along a close-packed Cu row.

- At the target position, the tip is again retracted by changing back to the imaging parameters. A subsequent image is taken to check if the manipulation was successful. While in general the manipulation efficiency strongly depends on the STM tip, decent tips yield a success rate of over 90%.

The image sequence displayed in Figure 2(d) presents some snapshots during the writing procedure of the letters CFI (short for Canada Foundation for Innovation). The high-resolution image in Figure 2(e) shows the final step of the manipulation process. Every blue spot is a single CO molecule adsorbed on an 'on top' position of the underlying Cu substrate lattice. Thus, for example the separation of two CO molecules in the letter 'I' is a mere 5 Å. The successful assembly and imaging of this artificial nanostructure demonstrates the high stability and performance of the low-temperature STM at UBC.

3 Supramolecular engineering

Figure 3 introduces a series of the molecular building blocks employed for our studies. On the one hand we apply the amino acid methionine to self-assemble highly regular nanogratings (Section 3.1). As illustrated in Figure 3(a) the neutral gas phase configuration of this small biological molecule is characterised by its functional groups (i.e., carboxylic and amino group) and the sulphur atom in the side chain. Due to their inherent importance for molecular recognition and self-assembly amino acids such as methionine represent an important class of building blocks for molecular architectures on surfaces [33–37]. Moreover, studying the interaction between biomolecules and solid surfaces is decisive for the development of biosensors or biocompatible materials [38–40].

Figure 3 Structural models of the functional building blocks applied for molecular self-assembly as discussed in this review. (a) The amino acid methionine in its neutral gas phase state with colour coded atoms: the length of the molecule along its side chain is around 8 Å. (b) Free base tetrapyridyl-porphyrin (H_2-TPyP). The arrows indicate a possible nonplanar distortion of the molecular core and a rotation of the *meso*-groups as discussed in the text. (c) Metalated tetraphenyl-porphyrin (M-TPP). The circles highlight the different endgroups, which control the self-assembly behaviour as it will be discussed in Section 3.2 (for colours see online version)

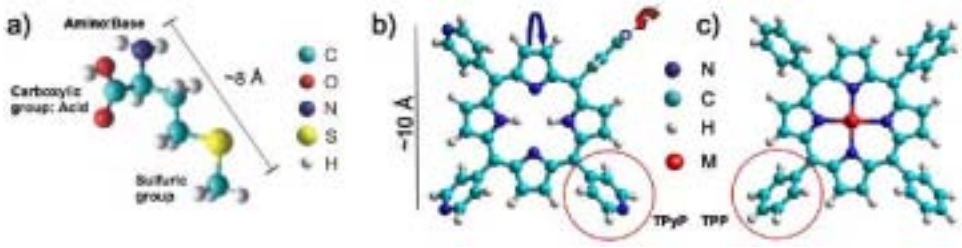

Porphyrins, as the second set of complex species under investigation, exhibit an intriguing variety of functional properties, which are exploited in both biological and artificial systems [41]. Thus, these versatile molecules are promising units to assemble functional layers and nanostructures on surfaces, specifically opening new opportunities

to build sensors, and nanoscale optical and magnetic materials [42,43]. As illustrated in Figure 3(b) and (c), the functionality and self-assembly of tetraarylporphyrins is based on three main features:

- The porphyrin core can host a wide range of metals, which present active sites to reversibly form porphyrin-ligand complexes [44,45].
- Porphyrins with a wide variety of *meso*-substituents can be synthesised. They co-determine the molecules' functional properties and render building blocks for metal-organic networks in solid state chemistry [46] and 2-D molecular engineering [3,47–52].
- The flexibility of the porphyrin core and the rotational degrees of freedom of the *meso*-groups allow for a conformational adaptation of the molecule to its local environment [48,53] and their considerate manipulation [20,54,55].

In Section 3.3 we present results on self-assembled porphyrin layers, address their molecular conformation, and report a molecular-level investigation on a novel scheme for the fabrication of metallo-porphyrins (Section 3.4).

3.1 Zwitterionic self-assembly of methionine on Ag(111)

Upon deposition of small methionine concentrations, STM observations show one-dimensional features on Ag(111) terraces, reflecting molecular self-assembly. This is illustrated by the image reproduced in Figure 4(a), taken for a coverage of å0.05 ML, showing 1D arrangements with discrete widths of 19 and 38 Å, respectively. Moreover, molecular chains exhibit striking extensions, for instance the length of the left methionine stripe exceeds 180 nm. Three different orientations are found which follow the close-packed <110> high-symmetry substrate orientations (cf. the inset in Figure 4(a) where the atomic structure of the Ag(111) lattice is depicted). This is a first indication that site-specific bonding at the surface is decisive in the observed methionine self-assembly scenario. The molecular surface concentration plays an important role in the mesoscopic ordering and domain formation of the molecular stripes. While at low concentrations any chain orientation along the close-packed of the substrate is equiprobable, beyond a critical coverage of å0.10 ML domains with mutual alignment appear (cf. Figure 4(b)), i.e., there is a mesoscopic ordering of the methionine stripes. In the data depicted in Figure 1(c) the interstripe distances are in the 85–190 Å range, and their correlated orientation signals repulsive long-range interactions (presumably resulting from the modified surface electronic structure in the presence of the molecular chains [4,56]).

Upon further increasing the coverage the mesoscopic ordering becomes more regular. Thus tunable and regular nanogratings can be fabricated. Figure 4(b) and (c) show two corresponding examples for coverages of å0.15 and å0.38 ML, respectively. In both preparations all stripes have a single width of 38 Å. The grating periodicity is 275 Å (standard deviation $\sigma \cong 40$ Å) in Figure 4(b) and 94 Å ($\sigma \cong 9$ Å) in Figure 4(c). Only with coverages exceeding approximately 0.65–0.70 ML, two-dimensional molecular islands evolve (cf. Figure 4(d)).

The nanogratings order in extended domains that can be as large as several tens of μm^2. An interesting application for these regular nanogratings with tunable spacing constant could be their use as templates for the design of functional linear arrangements

such as nanowires. The thermal stability of the nanogratings has been studied by STM for this purpose, the outcome being that they are stable up to room temperature, with molecular desorption occurring only above ~370 K.

Figure 4 Tuning the self-assembly of one dimensional methionine nanogratings. (a) STM image showing the extended one dimensional chains following the close-packed orientations of the substrate (I = 0.7 nA, U = –120 mV) at very low coverage (Θ ~ 0.05 ML). Inset: atomic resolution of Ag(111). (b) Chains aligned in parallel to form a grating with a periodicity of 275 Å ($\sigma \cong$ 40 Å, I = 0.8 nA, U = –800 mV, Θ ~ 0.15 ML). (c) 94 Å ($\sigma \cong$ 9 Å) periodicity (I = 0.1 nA, U = –500 mV, Θ ~ 0.38 ML). (d) Coalescing chains at higher coverage (I = 0.11 nA, U = –250 mV, Θ ~ 0.75 ML). (e) Histogram of the interchain spacing as function of the molecular coverage (for colours see online version)

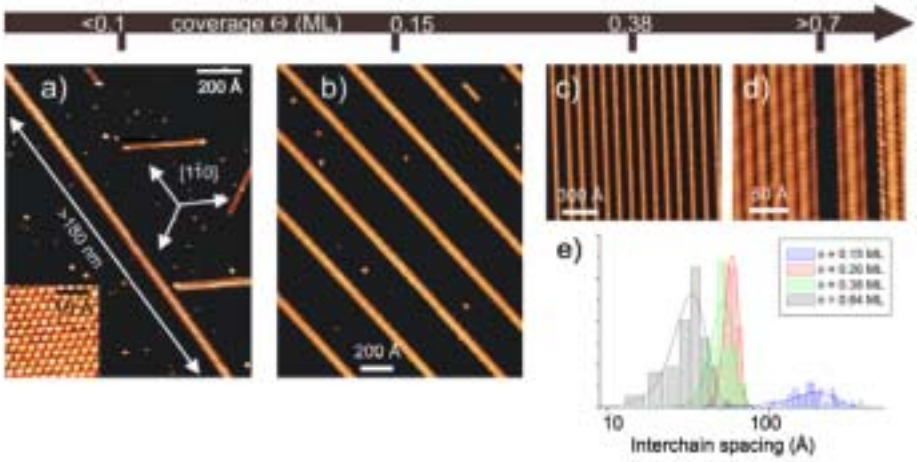

The high-resolution STM data in Figure 5(a) reveal the methionine positioning within the supramolecular structures. The stripes comprise elliptical features with a long axis of 8 Å, which corresponds to the dimension of a single molecule along its side-chain (cf. Figure 3(a)). Accordingly, these protrusions are identified with individual molecules bonding in a flat configuration to the surface. The long axis of the methionine ellipses encloses an angle of $60^{o} \pm 5^{o}$ with respect to the stripe orientation. Moreover, the separation between two adjacent molecules in this direction amounts to 5.8 Å. This corresponds to twice the Ag(111) surface lattice constant, i.e., the substrate atomic lattice also dictates the row periodicity. XPS measurements allow to clarify the chemical state of the amino acid moiety and show that it adsorbs in its zwitterionic state containing a positively charged ammonium group NH^{+}_{3} and a carboxylate group (COO^{-}) [56–58].

The molecular resolution data demonstrate that the methionine stripes consist of either double or quadruple molecular rows, where the methionine is oriented at specific angles with respect to the stripe direction. In both cases the same pairing scheme of the molecules can be discerned. This strongly indicates that the reactive amino groups mediate dimerisation. In Figure 5(a) we depict a tentative model for the parallel molecular configuration, where amino-amino dimerisation and lateral coupling is accomplished through hydrogen bonding involving the ammonium and carboxylate groups. A related zwitterionic bonding scheme was identified in the formation of layered amino acid crystals, where it is associated with appreciable bonding energies [59,60].

Figure 5 (a) High-resolution scanning tunnelling microscopy image of a twin chain segment stabilised by the zwitterionic-bond motif illustrated by the overlaid structural models (I = 0.9 nA, U = –80 mV). (b) Total energy map for two interacting methionine molecules in an antiparallel configuration obtained with molecular mechanics calculations. The colour scale indicates total energy of the system vs. the relative position (*x*, *y*) between the two molecules. This calculation confirms the amino dimerisation through zwitterionic bonding of self-complementary carboxylate and ammonium groups (adapted from [56]) (for colours see online version)

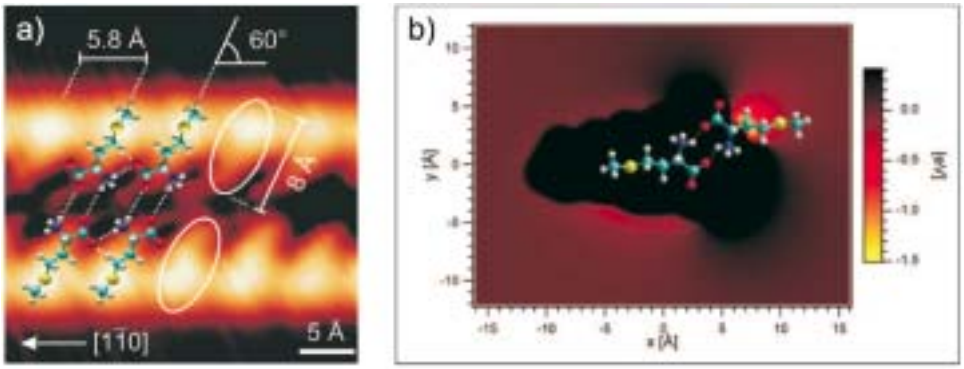

In order to corroborate the suggested zwitterionic 2D H-bonding scheme, molecular mechanics calculations were performed for a pair of methionine molecules confined onto a plane. Only molecule-molecule interactions were taken into account in these calculations, neglecting the influence of the Ag(111) substrate on the system. The molecules were taken in their zwitterionic state and conformational changes due to molecule-molecule interactions were not considered. The STM data demonstrate that the molecules lie flat on the substrate. We thus considered a system composed of two methionine zwitterions, with their geometry independently optimised. The total energy of the system was determined with respect to the relative position of the two molecules in the adsorption plane. The total energy map for the molecules in an antiparallel orientation (i.e., one molecule rotated by 180° on the adsorption plane with respect to the other) indicates that amino dimerisation involving the carboxylate and ammonium groups is energetically favourable, supporting our model (see Figure 5(b)). The length of the resulting dimer is 18 Å, which is in good agreement with the experimental data. The distance between an hydrogen atom of the ammonium group and an oxygen atom of the facing carboxylate group is 1.7 Å, which is in agreement with the hydrogen bond length of 3D amino acids [60]. Also results for the parallel configuration calculations show that lateral coupling proposed in our model is also energetically favourable [56].

3.2 Molecular superlattices for electron confinement

In the following we will discuss the application of methionine nanogratings to confine surface state electrons. Figure 6 gives an overview of the tunable confinement of the Ag(111) surface electrons by the use of a self-assembled methionine nanograting discussed above. The electronic structure of the pristine surface (Figure 6(a)) is illustrated by a STS dI/dV map overlaid on a constant current topograph to emphasise the standing wave pattern arising from the surface state electron scattering at atomic step edges [61,62]. The density of states (DOS) in large silver terraces resolved by STS (Figure 6(b))

shows the characteristic step-like feature (~67 meV below the Fermi level) due to the onset of the Shockley surface state band [63]. This 2D electron system is confined in one direction by a methionine superlattice. Figure 6(c) presents an STM topograph of an exemplary self-assembled grating with å6 nm periodicity. STS spectra taken between the molecular chains (Figure 6(d)) drastically differ from those of the free surface and comprise the peaked features typical of an electronic system confined in 1D [64].

Figure 6 (a) Topography of Ag(111) surface overlaid with a dI/dV STS map in order to enhance the standing wave pattern of the surface state electrons reflected at the step edges (I = 0.3 nA, U = 100 mV). (b) STS of the Ag surface state revealing the stepwise onset in the density of states typical for a 2D electron gas. (c) Regular methionine grating on Ag(111) self-assembled at room temperature (I = 0.1 nA, U = –500 mV). (d) Tunnelling spectrum taken in between the molecular chains demonstrating the 1D confinement of surface state electrons (adapted from [65]) (for colours see online version)

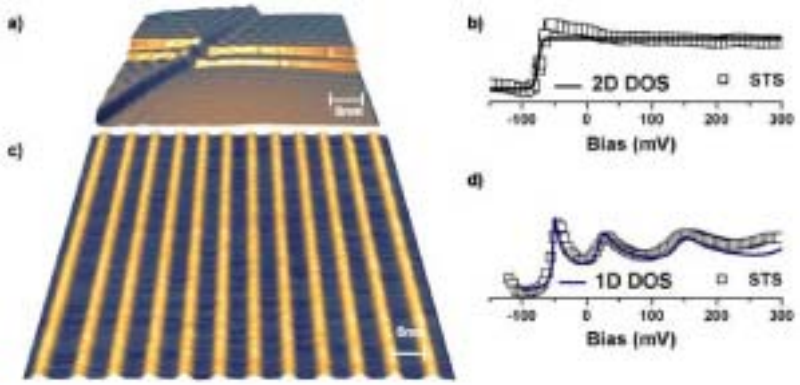

The data and analysis presented in Figure 7 detail the properties of the one-dimensional electronic confinement. The STM topograph in Figure 7(a), which clearly resolves the individual twin chains, depicts an element of a grating with 6.3 nm periodicity. In Figure 6(b) we show the corresponding differential conduction map obtained by measuring a series of tunnelling spectra in the voltage range –100 mV to 250 mV at 100 positions along the grating. The electronic ground level of the surface state at E_0 with its characteristic single node is clearly resolved. Similarly the energy quantisation and nodal structure of higher levels are directly visualised.

In order to rationalise the system's electronic properties the measured quantum confinement is modelled with a Fabry-Pérot interferometer [66]. For the quantification of the methionine boundaries' scattering properties we calculate the spatial variation of the surface DOS expressed as [65,66]:

$$\rho_{surf}(E,x) = \rho_b + \rho_{2D}/\pi \times \int_0^k \mathrm{d}q \frac{2}{\sqrt{k^2-q^2}} \frac{(1-r^2)[1+r^2+2r\,\cos(q\,L_{C1}+\varphi)\,\cos(q(L_{C1}-2x))]}{1+r^4-2r^2\,\cos(2q\,L_{C1}+2\varphi)},$$

where $k = \sqrt{2m^*(E-E_s)/\mathrm{Z}^2}$, L_{C1} is the effective resonator width, $\rho_{2D} = m^*/(\pi \mathrm{Z}^2)$ is the DOS of the pristine Ag(111) surface state electron gas, ρ_b is the bulk contribution to the DOS E_s is the bottom of the surface state band, r the reflectivity and φ the boundary

phase shift. Systematic parameter variation for a series of resonators revealed that the reflection plane for the methionine wires is located at centre of the molecular wire i.e., L_{C1} = 6.3 nm for the geometry in Figure 6. The parameters φ and r play a very different role allowing a confident separate fitting procedure of the data [66]. The positions of the peaks are strongly dependent on the boundary phase shift φ. Both peak broadening and oscillation amplitude depend predominantly on the reflection factor r. Altogether the features of our experimental data are quantitatively reproduced for $\varphi = -\pi$ and an energy dependent reflection factor, which was determined to be r å 0.85 at E_0 and follows an empirical 1/E decay law to reach r å 0.7 at E_2. The methionine boundary reflective characteristics are thus surprisingly similar to the ones reported for atomic step edges [66].

Figure 7 (a) High-resolution STM topograph of twin chain elements in a grating with individual methionine molecules resolved as rod-like protrusions (I = 0.1 nA, U = –500 mV). The indicated actual confinement length L_{C1} is larger than the topographic width of the Ag stripe and the effective scattering plane for the electrons, as derived from the modelling, is located at the centre of the wire. (b) Corresponding spatially resolved STS showing the first resonance of the surface state at E_0, and the energy level quantisation and spatial nodes for $E > E_0$. (c) The onset of the surface state can be continuously tuned by varying the molecular resonator width L_{C1} and follows an inverse square law (blue line, adapted from [65]) (for colours see online version)

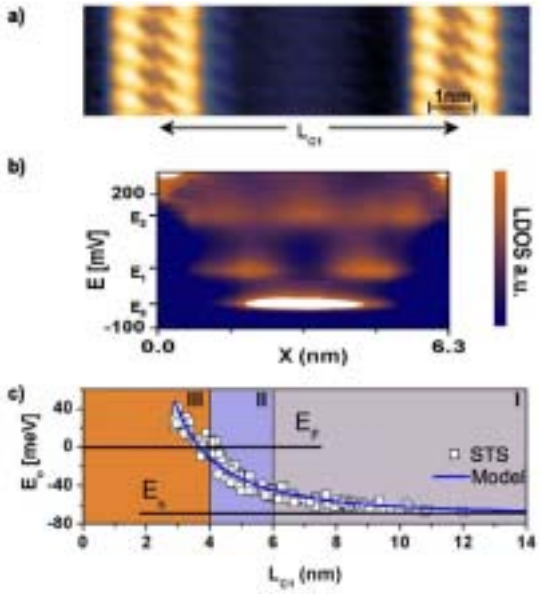

An essential feature of a quantum mechanical particle in a box model is that the energy levels obey an inverse quadratic dependence law on the confinement length. With the present self-assembled molecular resonators this can be verified systematically over a wide range. A compilation of an extensive data set where the surface state onset was extracted reveals that the confinement characteristics are similar in all self-assembly regimes described above and follow the expected law: $E_0 = (Z\pi)^2 / 2m^* L_{C1}^2 + E_S$, where E_S is the natural onset of the surface state energy band, and $m^* = 0.4\, m_e$ the corresponding electron effective mass. Note that for resonator widths $L_{C1} < 3.8$ nm the

first resonance is shifted above the Fermi level, i.e., the surface state is entirely depopulated, a behaviour similarly observed on narrow Ag(111) terraces [67].

3.3 Tetraarylporphyrins: self-assembly and conformation

Figure 8 shows STM images of the highly ordered layer structure resulting from H_2-TPyP deposition on Ag(111). The formation of large domains extended over hundreds of nm even at room temperature indicates a low diffusion barrier of H_2-TPyP on Ag(111). Accordingly, no single molecules can be immobilised even by lowering the substrate temperature to 100 K during deposition. One observes a staggered arrangement of clearly resolved molecular units. All molecules within a row following a given direction are oriented the same way, while this orientation switches in the neighbouring rows. Consequently, every second row shows the same molecular orientation. This characteristic pattern evolves in a wide substrate temperature range of 300–500 K. Figure 8(b) highlights the intramolecular features already detectable on the rather large scales of Figure 8(a). Besides the core with a depression in the centre, one can identify four protrusions forming a rectangle. From the molecular dimensions we assign each protrusion to one of the pyridyl legs. This is in agreement with the generally encountered parallel adsorption geometry of the porphyrin macrocycle on metal surfaces and indicates that the pyridyl groups are not oriented perpendicular to the molecular core (dihedral angle $\theta \neq 90°$). The corresponding models in Figure 8(b) clarify the structure and help to identify molecular features.

We describe this H_2-TPyP structure by a nearly rectangular unit cell with a molecule in every corner and a central molecule in a different azimuthal orientation. The unit cell parameters are as follows: $b_1 = 13.9 \pm 0.2$ Å, $b_2 = 27.4 \pm 0.2$ Å, $\beta = 93 \pm 2°$ [68].

By checking the registry of the H_2-TPyP overlayer with the subjacent Ag(111) substrate we conclude that the H_2-TPyP islands are not commensurate with the underlying Ag(111) substrate [68,69]. This means that not every equivalent molecule in the adlayer unit cell resides on an equivalent substrate lattice site. Accordingly, variations in the imaging height exist. A close look at Figure 8(a) shows a long-range intensity modulation, a quasi-hexagonal Moiré pattern with a periodicity of roughly 43 Å along the molecular rows. This indicates that the lateral intermolecular interactions dominate over site-specific adsorption on the smooth Ag(111) substrate.

The observed molecular packing is in accordance with results from elementary molecular mechanics calculations, which yield the parallel alignment of the corner molecules, while the central molecule has a different azimuthal orientation [68]. Thus, the lateral coupling mediated by the pyridyl groups seems to be decisive for the molecular packing. Accordingly, a phenyl terminated porphyrin species forms a square unit cell on Ag(111) exhibiting a single molecular orientation (see below).

After discussing the ordering of H_2-TPyP on Ag(111), we now address the imaging of the molecule's intramolecular features and its conformation. At negative sample bias voltages where the occupied states of the molecule contribute to the tunnelling current, the envelope of the molecules defines a rectangle (cf. Figure 8(b)). The reason for this deviation from a square-like geometry is that the pyridyl groups are alternately rotated out of the porphyrin plane, as depicted in Figure 3(b) and (c) [53,70]. This reduces the symmetry from square planar (D_{4h}) to D_{2d} and results in two different side lengths S1 and S2. To interpret the contrast mechanism we simulated STM images based on

semi-empirical extended Hueckel calculations in the framework of the HyperChem Package [71]. A constant electron density contour is obtained by integrating over the relevant molecular orbitals, which mimics a constant current STM image [72]. Similar methods relating calculated charge density maps of molecular orbitals to experimental STM data proved to be rather successful [73–76]. Also in our case, the general molecular appearance can be reproduced surprisingly well, despite ignoring the substrate: we get some intensity from the core and the legs have roughly the same apparent height (Figure 8(c), contributing molecular orbitals: HOMO to HOMO-6). These findings indicate that the molecular orbitals are not too strongly perturbed by the substrate electrons. Furthermore, the aspect ratio defined as S1/S2 depends sensitively on the orientation of the pyridyl legs. Consequently, one can employ these simulations in conjunction with the high resolution STM data to determine the molecular conformation. To do so, we calculate images for different dihedral angles θ, and extract the aspect ratios and compare them to the experimental observations. The best agreement is achieved for a dihedral angle of $60 \pm 5°$ (cf. Figure 8(d)). This value relates well to H_2-TPyP dihedral angle of ~62° in a solid state phase [77] or to θ of 63° determined by ab initio calculations for the ground state of a TPP molecule [48]. While a significant distortion of the porphyrin core is not consistent with our experimental data, a slight nonplanar deformation cannot be ruled out.

Figure 8 (a) The overview STM image of H_2-TPyP on Ag(111) shows that the molecules self-assemble in a staggered arrangement with two distinguishable rows (I = 0.8 nA, U = –300 mV). The inset (increased contrast) highlights the quasi-hexagonal Moiré pattern. (b) The high-resolution image allows to identify intramolecular features (I = 0.7 nA, U = –1.2 V): Besides the core with a depression in the centre, four protrusions corresponding to the legs are clearly discernible. The H_2-TPyP models including the unit cell (b_1, b_2) highlight the structure and facilitate the identification of core and terminal pyridyl groups. (c) STM image simulation based on the semiempirical extended Hückel method nicely reflects the rectangular shape of the molecule. (d) Molecular conformation of H_2-TPyP on Ag(111) as determined from a comparison of simulated images and high-resolution data: The dihedral angle θ equals $60 \pm 5°$ (adapted from [68]) (for colours see online version)

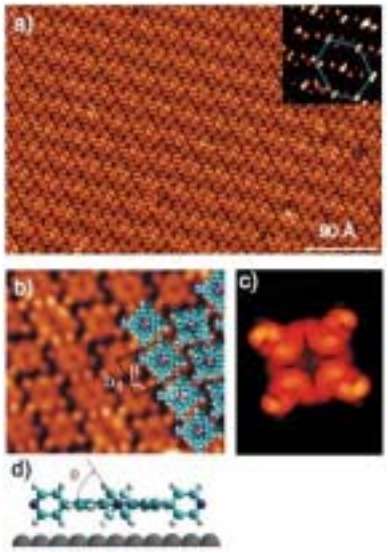

It is very instructive to study the impact of different substrates on the self-assembly and conformation of H_2-TPyP. Thus, after discussing the H_2-TPyP/Ag(111) case in quite some detail, we will briefly present some comparative results from the H2-TPyP/Cu(111) system. Figure 9(a) shows a Cu(111) terrace after deposition of a submonolayer coverage of H_2-TPyP at 300 K. One observes a random distribution of single H_2-TPyP molecules, which indicates that under these conditions H_2-TPyP is not mobile enough to form islands. This is in striking contrast to the high mobility of the very same molecule observed on Ag(111) (see Figure 8). The data reveal two bright protrusions in the centre of the molecule representing a strongly distorted molecular macrocycle. Before addressing this issue, we briefly discuss the adsorption site of H_2-TPyP on Cu(111). As mentioned in Section 2, CO molecules in a low coverage phase occupy exclusively 'on top' positions on the Cu(111) lattice. Additionally, H_2-TPyP and CO molecules can easily be imaged simultaneously by STM. Thus, CO molecules act as excellent markers to determine the adsorption site of H_2-TPyP on Cu(111). By matching a hexagonal grid representing the Cu(111) lattice with the position of the CO molecules, one can conclude that the H_2-TPyP molecules are centred on 'bridge' sites, irrespective of which of the three azimuthal orientations they follow [78]. Thus, H_2-TPyP clearly locks into a commensurate adsorption site on Cu(111), again in strong contrast from what was observed on the less reactive Ag(111) substrate.

Figure 9 (a) STM image of H_2-TPyP on Cu(111) upon adsorption at 300 K showing single, immobile and strongly distorted molecules. (b) Coexistence of H_2-TPyP with randomly distributed Fe momomers added in-situ at T < 10 K. (c) At T ~ 15 K Fe adatoms freely migrate and exclusively attach to the pyridyl groups of the stationary H_2-TPyP molecules. This points to the high affinity of the N containing ligands towards metal centres. The three main stages of this experiment are schematically illustrated in the column on the right (a, b, c same size, a: I = 0.35 nA, U = –1.1 V b: I = 0.2 nA, U = 30 mV, c: I = 0.2 nA, U = 20 mV) (adapted from [78]) (for colours see online version)

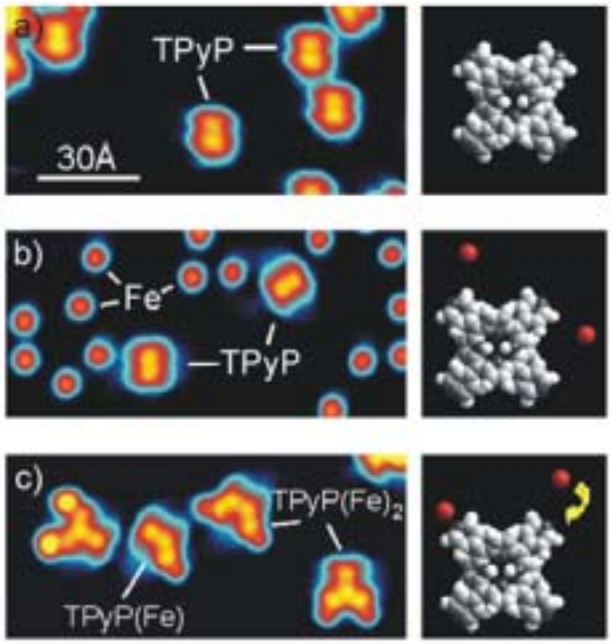

The strong binding of H_2-TPyP to Cu(111) seems to be triggered by a considerable interaction of the N containing pyridyl groups with Cu. Indeed the N adatoms are pulled towards the substrate, inducing a saddle shaped deformation of the macrocycle, which results in the two bright central lobes observed in the images [69,70,79]. Another hint pointing to the strong interaction between the terminal pyridyl groups and metal atoms comes from the experiment presented in Figure 9. In this case single Fe monomers were added in situ at cryogenic conditions (<10 K) (Figure 9(b)). At $T \sim 15$ K the Fe atoms start to move and are selectively captured by the pyridyl ligands of the stationary H_2-TPyP (Figure 9(c)) [78].

3.4 Controlled metalation of porphyrin nanoarrays

In the following we return to the system H_2-TPyP/Ag(111) to study a very different reaction scheme including the porphyrin macrocycle and metal centres: we examine the reactivity of the well defined H_2-TPyP precursor layer toward Fe atoms provided by an atomic beam (cf. Figure 10(a) and (b)). Upon exposure to minute amounts of Fe at 320 K the appearance of individual molecules changes drastically: STM images recorded at negative sample voltages show that a unique new species evolves, which is imaged brighter, with an increased apparent height of å0.7 Å compared to the H_2-TPyP precursor layer. Instead of the depression in the centre, this species exhibits a central rod-like protrusion (å12 Å long) which is always oriented along the molecular symmetry axis (here defined parallel to the short side of the rectangular envelope) and comprises two or three corrugation maxima. The number of modified molecules directly correlates with the Fe dose. Our data clearly reveal a preserved 2D TPyP layer structure, where exclusively the central porphyrin moieties undergo drastic changes. From now on we tentatively refer to the modified molecular species as Fe-TPyP.

Higher Fe doses allow the formation of regular Fe-TPyP arrays, where the alternating orientation of the Fe-induced features nicely reflects the orientation of the H_2-TPyP template layer (cf. Figure 10(b)). The apparent height of the Fe-TPyP molecules as well as the corrugation within the layer depends on the sample bias voltage. Under typical imaging conditions (U = –1 V) we measure an apparent height of 1.9 Å and a corrugation of 0.7 Å, respectively. Figure 10(d) shows height profiles along the molecular axis of two Fe-TPyP molecules in the same row. As mentioned before, between two and three protrusions are observed. This variation in the topographic appearance is due to the non-commensurability of the molecular layer on Ag(111) which induces subtle long-range height modulations as discussed above.

In order to investigate the nature of the Fe-TPyP molecules and to rationalise the origin of their drastically modified appearance in the STM topography we performed comparative experiments with Fe^{II}-tetraphenylporphyrin (Fe-TPP) layers self-assembled on Ag(111). TPP consists of a central porphyrin macrocycle and four terminal phenyl rings, and thus closely resembles TPyP. Each Fe-TPP comprises a Fe^{II} centre in the porphyrin plane (cf. inset Figure 10(c)) [80]. The self-assembly of this species on Ag(111) can be conducted with similar procedures as those employed for H_2-TPyP. An example for a highly regular Fe-TPP layer on Ag(111) is reproduced in the STM image in Figure 9(c). These data expose a striking similarity of the intramolecular features dominated by the porphyrin cores comprising the iron with the Fe-TPyP species shown in Figure 10(a) and (b). Again, the topographic appearance is dominated by two or

three protrusion along the molecular axis. The height profiles in Figure 10(e) accentuate this close resemblance.

Figure 10 (a) Exposing the H_2-TPyP precursor layer to a beam of Fe atoms drastically alters the shape of individual molecules. The apparent height of the modified species increases, resulting in a brighter appearance in the STM images. By increasing the Fe dose, their number can be tuned from zero to full saturation (b). As indicated by the unit cell, the molecular packing scheme remains unaffected by the reaction. (a: I = 0.85 nA, V = –300 mV, b: I = 0.65 nA, V = –400 mV,). (c) STM image of an Fe-TPP island exhibiting a molecular packing scheme described by a square unit cell with side lengths $b_1 = b_2 = 14.3 \pm 0.1$ Å (I = 0.65 nA, U = –0.8 V). The inset shows a model of a Fe-TPP molecule placed in the same azimuthal orientation as the Fe-TPP's in the STM image, the central Fe ion is coloured in red. The close resemblance to the topography of Fe-TPyP (b) is highlighted by the height profiles shown in (d) for Fe-TPyP and in (e) for Fe-TPP. Because of the non-commensurate nature of the porphyrin layers, a long-range height modulation of the molecular appearance is induced. As a consequence of the respective different substrate registries the porphyrin cores are imaged with two to three maxima along the molecular axis (adapted from [79]) (for colours see online version)

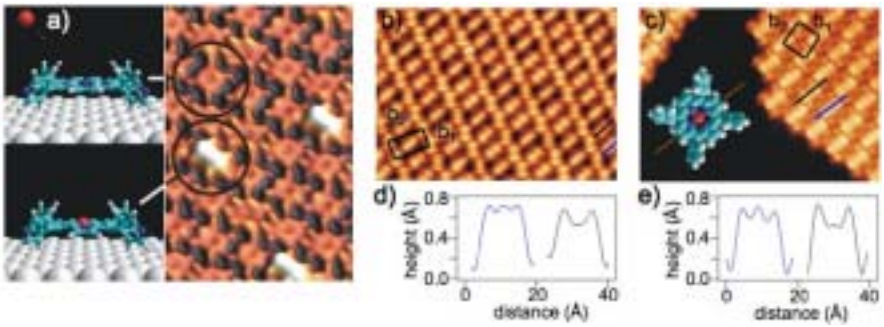

The data in Figure 10(c) reveal that regular Fe-TPP layers on Ag(111) exhibit a packing scheme with a correlated single azimuthal orientation of the molecules with respect to substrate high-symmetry directions. This distinction to the TPyP case arises from different lateral interactions due to a changed reactivity of the phenyl endgroups in comparison to the pyridyl substituents. The square unit cell (side length $b_1 = b_2 = 14.3 \pm 0.1$ Å) we observe agrees with observations of related metal-TPP molecules on close-packed noble metal surfaces [81,82].

The isostructural intramolecular features in the Fe-TPyP- and Fe-TPP-layers are a strong indication that in both cases genuine Fe^{II}-porphyrin species are present. The appearance of the Fe-porphyrins revealing an apparent symmetry break characterised by the pronounced protrusions along the molecular axis is associated with a nonplanar geometry of the porphyrin macrocycle. While undistorted porphyrin species feature a four-fold symmetric core appearance (cf. Figure 3(b) and (c)), nonplanar deformations result in pronounced protrusions establishing a two-fold symmetry of the porphyrin macrocycle [48,54,55,83]. Fe-tetraarylporphyrin species with a saddle shape are well-known and can serve as a tentative explanation of the observed features [84,85]. In this nonplanar deformation one opposing pair of pyrrole rings tilts up, while the other pair tilts down. Judging from the molecular dimensions the two outer protrusions originate from the upwards bent pyrrole pair, while the central protrusion relates to the Fe ion. The fact that the terminal groups are alternately rotated out of the porphyrin plane

allows only one pyrrole pair to tilt up, while the other pair is hindered by steric repulsion between hydrogen atoms of the ring and the terminal groups. Thus, we observe the protrusion exclusively along a specific symmetry axis in the 2-D porphyrin layers.

Figure 11 (a)–(c): Chemical sensitivity through bias-dependent imaging of H_2-TPyP and Fe-TPyP. The relative apparent height and appearance of H_2-TPyP and Fe-TPyP is strongly bias voltage dependent due to metalation induced modifications of the molecular electronic structure, as outlined in d and e. While the Fe-TPyP species appears brighter than H_2-TPyP at negative sample voltages (cf. Figure 10(a)), an inverted or vanishing contrast can be established by tuning the tunnelling voltage to specific positive values. The green circle highlights the position of one specific Fe-TPyP molecule (see text for full discussion). All three images are taken at a set point current of 0.71 nA. (d)–(e): Unoccupied electronic states of H_2-TPyP, Fe-TPyP and Fe-TPP: (d) Tunnelling spectra taken on bare Ag(111) patches show the pronounced step-like onset of the density of states at ~–67 meV associated with the surface state of the pristine substrate. The surface state is quenched upon H_2-TPyP adsorption, whereas a peak associated with the lowest lying unoccupied molecular orbitals (LUMOs) appears. The two spectra are shifted by a vertical offset for clarity. (e) The comparison of the H_2-TPyP with the Fe-TPyP and Fe-TPP tunnelling spectra reveals an energetic upward shift of the LUMOs which appear for both Fe-porphyrins at an energy of roughly 1000 meV. The plotted spectra represent a sum over several identical molecules as well as a spatial average over different spots on a molecule. The yellow arrows indicate the bias voltages used to acquire the images a), (b) and (c), respectively (adapted from [79]) (for colours see online version)

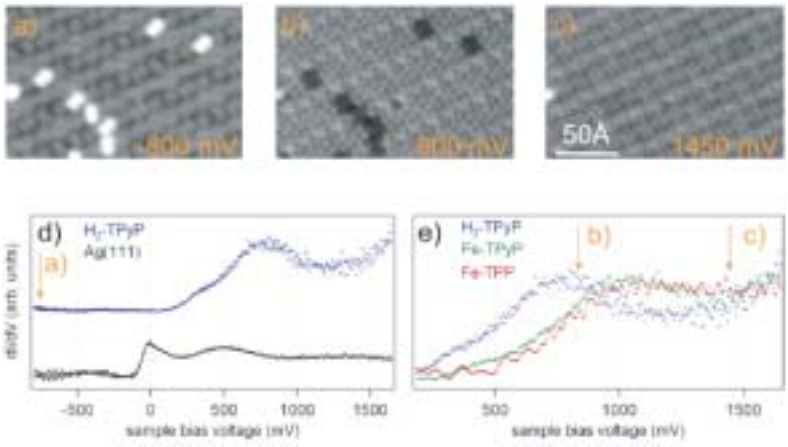

The conclusions drawn from the structural analysis are substantiated by STS observations which elucidate the electronic properties of the different (metallo-)porphyrin species. The data in Figure 11(d) reveal that the step-like increase in the STS spectra resulting from the onset of the Ag(111) surface state at an energy of –67 meV [86,87] disappears upon the formation of the pure H_2-TPyP layers. The latter exhibit rather a pronounced feature at +740 meV associated with the TPyP's two lowest unoccupied molecular orbitals (LUMOs), which are energetically very close in the isolated porphyrin molecule [88,89]. By contrast, the Fe-TPyP and Fe-TPP LUMO levels shown in Figure 11(e) are shifted towards higher energies and are found at 990 meV and 1020 meV, respectively. This upward shift is in agreement with spectroscopic observations [90] and theoretical calculations [89]. It arises from the interactions between the LUMOs and the filled d_π metal orbitals and has a direct impact on the topographic imaging of H_2-TPyP and

Fe-TPyP in constant current STM images (cf. Figure 11(a)–(c)). At negative sample voltages the Fe-TPyP molecules appear brighter than the H_2-TPyP species (cf. Figures 10(a) and 11(a)), while tuning the sample voltage to a positive value between the H_2-TPyP and Fe-TPyP LUMO energies results in a contrast inversion (Figure 11(b)), as the Fe-TPyP LUMO does not mediate electron tunnelling. At voltages well above the upshifted Fe-TPyP LUMO levels (Figure 11(c)) the two porphyrin species are essentially indistinguishable, in full agreement with the spectroscopic data. The voltage-dependent topography of Fe-TPP is very similar to that of Fe-TPyP. The almost identical LUMO shift for both Fe-TPyP and Fe-TPP (cf. Figure 11(e)) is ascribed to the fact that these molecular orbitals have major electron densities only at the porphyrin core [83], whence there energetics is hardly affected by the different *meso* substituents [49,89].

Thus both the structural analysis and the electronic structure characteristics of the three porphyrin species evidence a metalation reaction upon exposing adsorbed H_2-TPyP to Fe atoms. This implies that the metalloporphyrin formation readily occurs in situ on the surface. The methodology described is expected to provide a basis for the synthesis of high-purity metalloporphyrin nanostructures on surfaces, which could not be obtained by conventional methods as organic molecular beam epitaxy or deposition in solution, due to a limited thermal stability and/or high reactivity of specific metalloporphyrins.

4 Conclusions

Summarising, we expounded exemplary STM and STS studies addressing molecular recognition and self-assembly on metal surfaces. Following the demonstration of controlled manipulation on the atomic scale to build artificial nanostructures, we focussed on the self-assembly of highly ordered structures from functional molecular building blocks: Methionine on Ag(111) provides the possibility to realise extended biomolecular nanogratings with tunable periodicity. Notably we employed these stable gratings as confinement structures for surface state electrons. The analysis of tetraarylporphyrin layers reveals that STM is not only capable of imaging self-assembly characteristics, but also grants access to the molecular conformation and electronic structure of the adsorbed species. Furthermore we reported a new bottom-up approach for the fabrication of metallo-porphyrin architectures on surfaces via in situ metalation. The presented investigations illustrate that supramolecular design of low-dimensional materials on surfaces bears promise for nanotechnology.

Acknowledgements

Work supported by Canada Foundation for Innovation, British Columbia Knowledge and Development Fund, and the Canadian National Science and Engineering Research Council. Willi Auwärter and Alexander Weber-Bargioni acknowledge scholarships from Swiss National Science Foundation and Deutscher Akademischer Austauschdienst, respectively. We are grateful for fruitful collaborations and discussions with O. Gröning, R. Fasel, G. Sawatzky, T. Greber, S. Brink, M. Ruben, D. Cvetko, A. Cossaro and A. Morgante.

References and Notes

1 Lehn, J.M. (2002) 'Toward complex matter: supramolecular chemistry and self-organization', *Proc. Nat. Acad. Sci*., Vol. 99, pp.4763–4768.

2 Gates, B.D., Xu, Q., Stewart, M., Ryan, D., Willson, C.G. and Whitesides, G.M. (2005) 'New approaches to nanofabrication: molding, printing, and other techniques', *Chem. Rev.*, Vol. 105, p.1171.

3 Barth, J.V., Costantini, G. and Kern, K. (2005) 'Engineering atomic and molecular nanostructures on surfaces', *Nature*, Vol. 437, pp.671–679.

4 Barth, J.V. (2007) 'Molecular architectonic on metal surfaces', *Annu. Rev. Phys. Chem.*, Vol. 58, pp.375–407.

5 Binnig, G. and Rohrer, H. (1987) 'Scanning tunneling microscopy – from birth to adolescence', *Rev. Mod. Phys*., Vol. 59, pp.615–625.

6 Gimzewski, J.K. and Joachim, C. (1999) 'Nanoscale science of single molecules using local probes', *Science*, Vol. 283, pp.1683–1688.

7 Ho, W. (2002) 'Single-molecule chemistry', *J. Chem. Phys*., Vol. 117, pp.11033–11061.

8 Auwärter, W., Jahnz, G., Reichert, J., Weber-Bargioni, A., Schiffrin, A., Negulyaev, N., Stepanyuk, V.S. and Barth, J.V. (2007) unpublished.

9 Eigler, D.M. and Schweizer, E.K. (1990) 'Positioning single atoms with scanning tunneling microscope', *Nature*, Vol. 344, pp.524–526.

10 Stroscio, A.J. and Eigler, D.M. (1991) 'Atomic and molecular manipulation with the scanning tunneling microscope', *Science*, Vol. 254, pp.1319–1326.

11 Neu, B., Meyer, G. and Rieder, K.H. (1995) 'Controlled vertical and lateral manipulation of single atoms and small molecules with the scanning tunneling microscope', *Mod. Phys. Lett.*, Vol. 9, p.963.

12 Meyer, G. and Rieder, K.H. (1997) 'Controlled manipulation of single atoms and small molecules with the scanning tunneling microscope', *Surf. Sci.*, pp.1087–1093.

13 Bartels, L., Meyer, G. and Rieder, K.H. (1997) 'Controlled vertical manipulation of single CO molecules with the scanning tunneling microscope: a route to chemical contrast', *Appl. Phys. Lett.*, Vol. 71, p.213.

14 Jung, T.A., Schlittler, R.R., Gimewski, J.K., Tang, H. and Joachim, C. (1996) 'Controlled room-temperature positioning of individual molecules: molecular flexure and motion', *Science*, Vol. 271, pp.181–184.

15 Hla, S.W., Bartels, L., Meyer, G. and Rieder, K.H. (2000) 'Inducing all steps of chemical reaction with the scanning tunneling microscope tip: towards single molecule engineering', *Phys. Rev. Lett.*, 85, p.2777.

16 Piva, P.G., DiLabio, G.A., Pitters, J.L., Zikovsky, J., Rezeq, M., Dogel, S., Hofer, W.A. and Wolkow, R.A. (2005) 'Field regulation of single-molecule conductivity by a charged surface atom', *Nature*, Vol. 435, p.658.

17 Moresco, F., Meyer, G., Rieder, K-H., Tang, H., Gourdon, A. and Joachim, C. (2001) 'Conformational changes of single molecules induced by scanning tunneling microscopy manipulation: a route to molecular switching', *Phys. Rev. Lett.*, Vol. 86, p.672.

18 Moresco, F., Meyer, G. and Rieder, K-H. (2001) 'Low temperature manipulation of big molecules in constant height mode', *Appl. Phys. Lett.*, Vol. 78, pp.306–308.

19 Lagoute, J., Kanisawa, K. and Fölsch, S. (2004) 'Manipulation and adsorption-site mapping of single pentacene molecules on Cu(111)', *Phys. Rev. B*, Vol. 70, p.245415-1-6.

20 Loppacher, C., Guggisberg, M., Pfeiffer, O., Meyer, E., Bammerlin, M., Luthi, R., Schlittler, R., Gimzewski, J.K., Tang, H. and Joachim, C. (2003) 'Direct determination of the energy required to operate a single molecule switch', *Phys. Rev. Lett.*, Vol. 90, p.066107-1-4.

21 Otero, R., Rosei, F. and Besenbacher, F. (2006) 'Scanning tunneling microscopy manipulation of complex organic molecules on solid surfaces', *Annu. Rev. Phys. Chem.*, Vol. 57, pp.497–525.

22 Crommie, M.F., Lutz, C.P. and Eigler, D.M. (1993) 'Confinement of electrons to quantum corrals on a metal surface', *Science*, Vol. 262, p.218.

23 Kliever, J., Berndt, R. and Crampin, S. (2000) 'Controlled modification of individual adsorbate electronic structure', *Phys. Rev. Lett.*, Vol. 85, pp.4936–4939.

24 Nazin, G.V., Qiu, X.H. and Ho, W. (2003) 'Visualization and spectroscopy of a metal-molecule-metal bridge', *Science*, Vol. 302, pp.77–81.

25 Grill, L., Rieder, K-H., Moresco, F., Stojkovic, S., Gourdon, A. and Joachim, C. (2005) 'Controlling the electronic interaction between a molecular wire and its atomic scale contacting pad', *Nano Lett.*, Vol. 5, pp.859–863.

26 Rosei, F., Schunack, M., Jiang, P., Gourdon, A., Laegsgaard, E., Stensgaard, I., Joachim, C., Besenbacher, F. (2002) 'Organic molecules acting as templates on metal surfaces', *Science*, Vol. 296, pp.328–331.

27 Fölsch, S., Hyldgaard, P., Koch, R. and Ploog, K.H. (2004) 'Quantum confinement in monoatomic Cu chains on Cu(111)', *Phys. Rev. Lett.*, Vol. 92, p.056803-1-4.

28 Bartels, L., Meyer, G. and Rieder, K.H. (1997) 'Basic steps involved in the lateral manipulation of single CO molecules and rows of CO molecules', *Chem. Phys. Lett.*, Vol. 273, p.371.

29 Bartels, L., Meyer, G. and Rieder, K.H. (1997) 'Basic steps of lateral manipulation of single CO molecules and diatomic clusters with a scanning tunneling microscope tip', *Phys. Rev. Lett.*, Vol. 79, p.697.

30 Heinrich, A.J., Lutz, C.P., Gupta, J.A. and Eigler, D.M. (2002) 'Molecule cascades', *Science*, Vol. 298, p.1381.

31 Nieminen, J.A., Niemi, E. and Rieder, K.H. (2004) 'Interference between competing tunneling channels and chemical resolution of STM', *Surf. Sci.*, Vol. 552, pp.L47–L52.

32 Persson, M. (2004) 'Theory of elastic and inelastic tunneling microscopy and spectroscopy: CO on Cu revisited', *Philos. Trans. R. Soc. London, A*, Vol. 362, pp.1173–1183.

33 Kawai, T., Tanaka, H. and Nakagawa, T. (1997) 'Low dimensional self-organization of DNA-base molecules on Cu(111) surfaces', *Surf. Sci.*, Vol. 386, pp.124–136.

34 Kühnle, A., Linderoth, T.R., Hammer, B. and Besenbacher, F. (2002) 'Chiral recognition in dimerization of adsorbed cysteine observed by scanning tunneling microscopy', *Nature*, Vol. 415, pp.891–893.

35 Chen, Q. and Richardson, N.V. (2003) 'Enantiomeric interactions between nucleic acid bases and amino acids on solid surfaces', *Nat. Mater.*, Vol. 2, pp.324–328.

36 Otero, R., Schöck, M., Molina, L.M., Laegsgaard, E., Stensgaard, I., Hammer, B. and Besenbacher, F. (2004) 'Guanine quartet networks stabilized by cooperative hydrogen bonds', *Angew. Chem., Int. Ed.*, Vol. 44, pp.2–6.

37 Kelly, R.E.A. and Kantorovich, L.N. (2006) 'Planar nucleic acid base super-structures', *J. Mater. Chem.*, Vol. 16, pp.1894–1905.

38 Kasemo, B. (2002) 'Biological surface science', *Surf. Sci.*, Vol. 500, pp.656–677.

39 Sarikaya, M., Tamerler, C., Jen, A.K.Y., Schulten, K. and Baneyx, F. (2003) 'Molecular biomimetics: nanotechnology through biology', *Nat. Mater.*, Vol. 2, pp.577–585.

40 Preuss, M., Schmidt, W.G. and Bechstedt, F. (2005) 'Coulombic amino group-metal bonding: adsorption of adenine on Cu(110)', *Phys. Rev. Lett.*, Vol. 94, p.236102.

41 Dolphin, D. (Ed.) (1978) *The Porphyrins*, Academic Press, New York.

42 Kadish, K.M., Schmith, K.M. and Guilard, R. (Eds.) (2000) *The Porphyrin Handbook Vol. 6, Applications: Past, Present and Future*, Academic Press, San Diego.

43 Elemans, J.A.A.W., Hameren, R.v., Nolte, R.J.M. and Rowan, A.E. (2006) 'Molecular materials by self-assembly of porphyrins, phthalocyanines, and perylenes', *Adv. Mater*., Vol. 18, pp.1251–1266.

44 Williams, F.J., Vaughan, O.P.H., Knox, K.J., Bambos, N. and Lambert, R.M. (2004) 'First observation of capping/uncapping by a ligand of a Zn porphyrin adsorbed on Ag(100)', *Chem. Commun*., p.1688.

45 Shoji, O., Tanaka, H., Kawai, T. and Kobuke, Y. (2005) 'Single molecule visualization of coordination-assembled porphyrin macrocycles reinforced with covalent linkings', *J. Am. Chem. Soc*., Vol. 127, pp.8598–8599.

46 Kosal, M.E. and Suslick, K.S. (2000) 'Microporous porphyrin and metalloporphyrin materials', *J. Solid State Chem*., Vol. 152, p.87.

47 Kunitake, M., Batina, N. and Itaya, K. (1995) 'Self-organized porphyrin array on iodine-modified Au(111) in electrolyte solutions: in situ scanning tunneling microscopy study', *Langmuir*, Vol. 11, p.2337.

48 Yokoyama, T., Yokoyama, S., Kamikado, T. and Mashiko, S. (2001) 'Nonplanar adsorption and orientational ordering of porphyrin molecules on Au(111)', *J. Chem. Phys.*, Vol. 115, p.3814.

49 Scudiero, L., Barlow, D.E. and Hipps, K.W. (2002) 'Scanning tunneling microscopy, orbital-mediated tunneling spectroscopy, and ultraviolet photoelectron spectroscopy of nickel(II) octaethylporphyrin deposited from vapor', *J. Phys. Chem. B*, Vol. 106, pp.996–1003.

50 Bonifazi, D., Spillmann, H., Kiebele, A., Wild, M.d., Seiler, P., Cheng, F., Güntherodt, H-J., Jung, T. and Diederich, F. (2004) 'Supramolecular patterned surfaces driven by cooperative assembly of C60 and porphyrins on metal substrates', *Angew. Chem., Int. Ed.*, Vol. 43, pp.4759–4763.

51 Abel, M., Oison, V., Koudia, M., Maurel, C., Katan, C. and Porte, L. (2006) 'Designing a new two-dimensional molecular layout by hydrogen bonding', *ChemPhysChem*, Vol. 7, pp.82–85.

52 Hipps, K.W., Scudiero, L., Barlow, D.E. and Cooke, M.P. (2002) 'A self-organized 2-dimensional bifunctional structure formed by supramolecular design', *J. Am. Chem. Soc*., p.124.

53 Jung, T.A., Schlittler, R.R. and Gimewski, J.K. (1997) 'Conformational identification of individual adsorbed molecules with the STM', *Nature*, Vol. 386, p.696.

54 Qiu, X.H., Nazin, G.V. and Ho, W. (2004) 'Mechanisms of reversible conformational transitions in a single molecule', *Phys. Rev. Lett*., Vol. 93, p.196806.

55 Iancu, V., Deshpande, A. and Hla, S-W. (2006) 'Manipulating Kondo temperature via single molecule switching', *Nano Lett*., Vol. 6, pp.820–823.

56 Schiffrin, A., Riemann, A., Auwärter, W., Pennec, Y., Weber-Bargioni, A., Cvetko, D., Cossaro, A., Morgante, A. and Barth, J.V. (2007) 'Zwitterionic self-assembly of L-methionine nanogratings on the Ag(111) surface', *PNAS*, Vol. 104, pp.5279–5284.

57 Löfgren, P., Krozer, A., Lausmaa, J. and Kasemo, B. (1997) 'Glycine on Pt(111): a TDS and XPS study', *Surf. Sci*., Vol. 370, pp.277–292.

58 Gonella, G., Terreni, S., Cvetko, D., Cossaro, A., Mattera, L., Cavalleri, O., Rolandi, R., Morgante, A. and Floreano, L. (2005) 'Ultrahigh vacuum deposition of L-cysteine on Au(110) studied by high-resolution X-ray photoemission: from early stages of adsorption to molecular organization', *J. Phys. Chem. B*, Vol. 109, pp.18003–18009.

59 Dalhus, B. and Görbitz, C.H. (1999) 'Molecular aggregation in selected crystalline 1 : 1 complexes of hydrophobic D- and L-amino acids. II. The D-norleucine series', *Acta Cryt*., Vol. C55, pp.1105–1112.

60 Dalhus, B. and Görbitz, C.H. (2004) 'Crystal structures of hydrophobic amino acids: interaction energies of hydrogen-bonded layers revealed by ab initio calculations', *J. Mol. Struct. (Theochem)*, Vol. 675, pp.47–52.

61 Crommie, M.F., Lutz, C.P. and Eigler, D.M. (1993) 'Imaging standing waves in a two-dimensional electron gas', *Nature*, Vol. 363, pp.524–527.

62 Hasegawa, Y. and Avouris, P. (1993) 'Direct observation of standing wave formation at surface steps using STS', *Phys. Rev. Lett*., Vol. 71, p.1071.

63 Li, J., Schneider, W-D. and Berndt, R. (1997) 'Local density of states from spectroscopic scanning tunneling microscope images: Ag(111)', *Phys. Rev. B*, Vol. 56, p.7656.

64 Avouris, P. and Lyo, I-W. (1993) 'Observation of quantum size effects at room temperature on metal surfaces with STM', *Science*, Vol. 264, pp.942–945.

65 Pennec, Y., Auwärter, W., Schiffrin, A., Weber-Bargione, A., Riemann, A. and Barth, J.V. (2007) 'Supramolecular gratings for tuneable confinement of electrons on metal surfaces', *Nat. Nanotechnol.*, Vol. 2, pp.99–103.

66 Bürgi, L., Jeandupeux, O., Hirstein, A., Brune, H. and Kern, K. (1998) 'Confinement of surface state electrons in Fabry-Perot resonator', *Phys. Rev. Lett*., Vol. 81, p.5370.

67 Morgenstern, K., Braun, K.F. and Rieder, K.H. (2002) 'Surface state depopulation on small Ag(111) terraces', *Phys. Rev. Lett.*, Vol. 89, p.226801.

68 Auwärter, W., Weber-Bargioni, A., Riemann, A., Schiffrin, A., Groening, O., Fasel, R. and Barth, J.V. (2006) 'Self-assembly and conformation of tetrapyridyl-porphyrin molecules on Ag(111)', *J. Chem. Phys*., Vol. 124, p.194708.

69 Weber-Bargioni, A., Auwärter, W., Schiffrin, A. and Barth, J.V. (2007) 'Temperature-dependent conformation, electronic structure and metallosupramolecular organization of tetrapyridyl porphyrin molecules on the Cu(111) surface', subm.

70 Yokoyama, T., Yokoyama, S., Kamikado, T. and Mashiko, S. (2001) 'Nonplanar adsorption and orientational ordering of porphyrin molecules on Au(111)', *J. Chem. Phys*., Vol. 115, p.3814.

71 HYPERCHEM, Hypercube Inc., 1115 NW 4th street, Gainesville, Florida 32601.

72 Gröning, O. and Fasel, R. (2004) *STM Generator Software*, EMPA Materials Science and Technology, Thun, Switzerland.

73 Lippel, P.H., Wilson, R.J., Miller, M.D., Wöll, C. and Chiang, S. (1988) 'High-resolution imaging of copper-phthalocyanine by scaning-tunneling microscopy', *Phys. Rev. Lett*., Vol. 62, pp.171–174.

74 Hallmark, V.M., Chiang, S., Meinhardt, K-P. and Hafner, K. (1993) 'Observation and calculation of internal structure in scanning tunneling microscopy images of related molecules', *Phys. Rev. Lett*., Vol. 70, pp.3740–3743.

75 Sautet, P. (1997) 'Images of adsorbates with the scanning tunneling microscope: theoretical approaches to the contrast mechanism', *Chem. Rev*., Vol. 97, pp.1097–1116.

76 Fasel, R., Parschau, M. and Ernst, K-H. (2006) 'Amplification of chirality in two-dimensional enantiomorphous lattices', *Nature*, Vol. 439, pp.449–452.

77 Silvers, S.J. and Tulinsky, A. (1967) 'The crystal and molecular structure of triclinic tetraphenylporphyrin', *J. Am. Chem. Soc*., Vol. 89, p.3331.

78 Auwärter, W., Klappenberger, F., Weber-Bargioni, A., Schiffrin, A., Strunskus, T., Wöll, C., Pennec, Y., Riemann, A. and Barth, J.V. (2007) 'Conformational adaptation and selective adatom capturing of tetrapyridyl-porphyrin molecules on a copper (111) surface', *J. Am. Chem. Soc*., Vol. 129, p.11279.

79 Auwärter, W., Weber-Bargioni, A., Brink, S., Riemann, A., Schiffrin, A., Ruben, M. and Barth, J.V. (2007) 'Controlled metalation of self-assembled porphyrin nanoarrays in two dimensions', *ChemPhysChem*, Vol. 8, pp.250–254.

80 Collman, J.P., Hoard, J.L., Kim, N., Lang, G. and Reed, C.A. (1975) 'Synthesis, stereochemistry, and structure-related properties of α,β,γ,δ-Tetraphenylporphinatoiron(II)', *J. Am. Chem. Soc*., Vol. 97, pp.2676–2681.

81 Scudiero, L., Barlow, D.E. and Hipps, K.W. (2000) 'Physical properties and metal ion specific scanning tunneling microscopy images of metal(II) tetraphenylporphyrins deposited from vapor onto gold (111)', *J. Phys. Chem. B*, Vol. 104, p.11899.

82 Suto, K., Yoshimoto, S. and Itaya, K. (2003) 'Two-dimensional self-organization of phthalocyanine and porphyrin: dependence on the crystallographic orientation of Au)', *J. Am. Chem. Soc*., Vol. 125, pp.14976–14977.

83 Weber-Bargioni, A., Auwärter, W., Schiffrin, A., Pennec, Y. and Barth, J.V. (2008) 'Visualizing the frontier orbitals of a conformationally adapted metalloporphyrin', *ChemPhysChem*, DOI: 10.1002/cphc.200700600, Vol. 9, pp.89–94.

84 Shelnutt, J.A., Song, X-Z., Ma, J.G., Jia, S-L., Jentzen, W. and Medforth, C.J. (1998) 'Nonplanar porphyrins and their significance in proteins', *Chem. Soc. Rev*., Vol. 27, pp.31–41.

85 Marques, H.M. and Brown, K.L. (2002) 'Molecular mechanics and molecular dynamics simulations of porphyrins, metalloporphyrins, heme proteins and cobalt corrinoids', *Coord. Chem. Rev*., Vol. 225, pp.123–158.

86 Li, J., Schneider, W-D., Berndt, R., Bryant, O.R. and Crampin, S. (1998) 'Surface-state lifetime measured by scanning tunneling microscopy', *Phys. Rev. Lett*., Vol. 81, pp.4464–4467.

87 Reinert, F., Nicolay, G., Schmidt, S., Ehm, D. and Hüfner, S. (2001) 'Direct measurements of the L-gap surface states on the (111) face of noble metals by photoelectron spectroscopy', *Phys. Rev. B*, Vol. 63, p.115415.

88 Lamoen, D. and Parrinello, M. (1996) 'Geometry and electronic structure of porphyrins and porphyrazines', *Chem. Phys. Lett*., Vol. 248, pp.309–315.

89 Liao, M-S. and Scheiner, S. (2002) 'Electronic structure and bonding in metal porphyrins, metal=Fe, Co,Ni, Cu, Zn', *J. Chem. Phys*., Vol. 117, pp.205–219.

90 Suslick, K.S. and Watson, R.A. (1992) 'The photochemistry of chromium, manganese, and iron porphyrin complexes', *New. J. Chem*., Vol. 16, pp.633–642.